INTERNATIONAL JOURNAL OF COMPUTERS COMMUNICATIONS & CONTROL
Online ISSN 1841-9844, ISSN-L 1841-9836, Volume: 19, Issue: 6, Month: December, Year: 2024
Article Number: 6857, https://doi.org/10.15837/ijccc.2024.6.6857

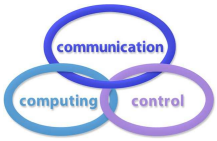

CCC Publications

H_∞- Static Output Feedback based Load Frequency Control of an Interconnected Power System with Regional Pole Placement

Srikanth Bondalapati, Rajeeb Dey, Cornel Barna, Valentina Emilia Balas

Srikanth Bondalapati
Department of Electrical Engineering
National Institute of Technology Silchar, Assam
*Corresponding author: srikanth21_rs@ee.nits.ac.in

Rajeeb Dey
Department of Electrical Engineering
National Institute of Technology Silchar, Assam
*Corresponding author: rajeeb@ee.nits.ac.in

Cornel Barna
Aurel Vlaicu University of Arad, Romania
*Corresponding author: cornel.barna@contactp.ro

Valentina Emilia Balas
Aurel Vlaicu University of Arad, Romania
balas@drbalas.ro

Abstract

This paper presents the design of an H_∞-based Restricted Static Output Feedback (RSOF) controller with regional pole placement in Linear Matrix Inequality (LMI) framework for Load Frequency Control (LFC) of a 2-area Interconnected Power System (IPS). The motivation behind the RSOF controller is to develop a controller with a predefined structure for implementing centralized and decentralized control strategy as per need. In this work a new stabilization criterion is developed by choosing circle and strip LMI regions for pole-placement along with the use of Particle Swarm Optimization (PSO) technique to tune the scalar parameters for the feasibility of the developed LMI criterion. The designed controller (both centralized and decentralized structure) with the above modifications improves the transient response of the frequency output. The designed controller is tested on a 2-area LFC model incorporating both conventional and renewable energy sources. Simulation results validate the effectiveness of the designed controller in attenuating disturbance and also enhancing the transient response. Also, simulation studies are carried out to test the robustness against time delays and cyberattacks. A comparative analysis is presented for various controllers, highlighting their performance differences.

Keywords: Load Frequency Control (LFC), Restricted SOF controller, Pole Placement, particle swarm optimization (PSO).

1 Introduction

Interconnected power systems (IPS) are constantly being upgraded to include renewable energy sources (RES) like wind and solar [1]. These RES help reduce carbon emissions. However, adding many wind and solar generators to IPS causes significant fluctuations in power generation. These fluctuations when combined with the load changes increases the imbalance between generation and demand that leads to frequency deviation in the power grid from the normal limit. Thus, Load Frequency Control (LFC) is essential to manage the frequency changes that eventually maintains the balance between power generation and demand in the IPS.

Many controller models have been studied in the field of LFC for IPS. These include robust PI controllers [2], [3], sliding mode controllers (SMC) [4, 5, 6], model predictive controllers (MPC) [7], PID controllers [8], and state feedback control [9]. PI controllers and their variants are widely used in industry because of their simple design, however to handle the uncertainties and disturbances, the controller gains are tuned using metaheuristic approaches [10, 11, 12, 13]. These metaheuristic approaches for PI designs are effective but suffers from the drawbacks of analytical tractability of the algorithms, computational burden and implementation issues in real-time power systems due to involvement of many slack variables that are not related with the system dynamics or power system parameters. In contrast the state-space mathematical models of LFC uses Lyapunov based controller design methods that has the advantages of the tractability of the design, ease of computation while handling different types of system complexities, uncertainties and constraints. The authors are referred to some important LMI-based design and tuning of controller methods from [9, 8, 14, 15, 16].

State feedback control design [17, 9] is not practical due to the requirement of all the state information to be feedback to the controller. This design is not viable economically, computationally and for physical realizability. While, output feedback controller design [18, 19] instead uses partial state information for computing the controller gain. But the design of output feedback controller is computationally challenging in terms of computing control gains that can give better performance with limited state information. For a large scale system (in this case multi-area IPS) where various subsystems (rather power system areas) are spread out over a large geographical area having many state information designing a centralised control scheme may lead various operational, computational and communication problems. As opposed to centralised control, decentralized control collects state information of the local power system area to have individual controllers for each power system area [6, 20].

The work in this paper is motivated from the work reported on restricted static output feedback (RSOF) controller to design a decentralised control scheme [21] and [22]. The method presented in these literature requires decomposition of the diagonal and off-diagonal terms of the Lyapunov matrices in order to obtain predefined control gain matrix. It is worth mentioning at this stage that, the design in [21] and [22] uses a decomposition technique that requires controller gain matrices to be purely square. This square structure constraint in-turn imposes limit on the selection of number of outputs that consequently affects the solvability of the LMI conditions for large scale systems.

The inherent structural shortcoming discussed above about the design methods presented in [21] and [22] restricts one to implement the results as it is for stabilising and enhancing the dynamic performance of any large-scale system. Thus, the design in [21] and [22] needs modifications in terms of an appropriate LMI region to place the closed loop poles to circumvent the inherent structural restrictions of the reported design. The novelty of this work lies in reporting the inherent shortcomings of the design methods in [21] and [22] for any large scale system and thereby point out the source of modification to obtain computationally feasible solution that can stabilise as well as enhance the dynamic performance of any large sacle system. In this work, first a 2-area LFC system model with renewable energy sources is proposed as a large scale system and secondly following the method in [22] a RSOF controller is designed with an appropriate combination of circular and strip LMI regions for pole-placement ensuring a feasible design a the large-scale system. Further, the current design uses a PSO-based metaheuristic optimization algorithm to tune the arbitrary scalar parameters involved in the LMI constraints unlike the use of "fminsearch" algorithm used in [22] with a suitable objective function.

The proposed controller design is implemented in a large-scale interconnected power system model

to show the efficacy of the design and it is compared with the results reported in [14, 15]. Additionally, robustness studies are conducted to assess the proposed controllers' effectiveness in managing time delays and cyberattacks [24] and [25].

The paper is organized as follows: The introduction provides an overview of the study. System Model and Description detail the system's mathematical model. H_∞ Controller Design covers the design and optimization of the controller. Simulation Results presents and analyzes the simulation outcomes. The conclusion summarizes the findings and suggests future work.

Table 1: Notations Used in the Paper

Notation	Description
$X = X^T > 0$	Positive definite symmetric matrix
$X_Q = X_Q^T$	Symmetric matrix X_Q
X^T	Transpose of a matrix X
$\mathcal{N}(\cdot)$	Null space of a matrix
$\mathcal{R}(\cdot)$	Range space of a matrix
$*$	Symmetric component in the matrix

2 System Model and Description

This section describes the state space model of the considered large-scale interconnected power systems with conventional sources and renewable energy sources (wind, PV). A two-area LFC scheme of the IPS is considered here, as shown in Fig. 1. One area has a wind energy source along with a conventional source while the second area is connected with a PV source along with a conventional source. Wind or solar power generation and changes in the power demand are considered as a disturbance to the IPS. The dynamical equations representing the LFC system are given in (1) - (11).

$$\Delta\dot{f}_1(t) = -\frac{1}{T_{p1}}\Delta f_1(t) + \frac{k_{p1}}{T_{p1}}\Delta P_{t1}(t) + \frac{k_{p1}}{T_{p1}}\Delta P_{WTG}(t) - \frac{k_{p1}}{T_{p1}}\Delta P_{d1}(t) - \frac{k_{p1}}{T_{p1}}\Delta P_{Tie}(t) \tag{1}$$

$$\Delta\dot{P}_{t1}(t) = -\frac{1}{T_{t1}}\Delta P_{t1}(t) + \frac{1}{T_{t1}}\Delta P_{g1}(t) \tag{2}$$

$$\Delta\dot{P}_{g1}(t) = -\frac{1}{R_1 T_{g1}}\Delta f_1(t) - \frac{1}{T_{g1}}\Delta P_{g1}(t) + \frac{1}{T_{g1}}\int ACE_1(t) + \frac{1}{T_{g1}}u_1(t) \tag{3}$$

$$\int \dot{ACE}_1(t) = B_1\Delta f_1(t) + \Delta P_{Tie}(t) \tag{4}$$

$$\Delta\dot{P}_{WTG}(t) = -\frac{1}{T_{WTG}}\Delta P_{WTG}(t) + \frac{1}{T_{WTG}}\Delta P_W(t) \tag{5}$$

$$\Delta\dot{P}_{Tie}(t) = 2\pi T_{12}\Delta f_1(t) - 2\pi T_{12}\Delta f_2(t) \tag{6}$$

$$\Delta\dot{f}_2(t) = -\frac{1}{T_{p2}}\Delta f_2(t) + \frac{k_{p2}}{T_{p2}}\Delta P_{t2}(t) + \frac{k_{p2}}{T_{p2}}\Delta P_{PV}(t) - \frac{k_{p2}}{T_{p2}}\Delta P_{d2}(t) + \frac{k_{p2}}{T_{p2}}\Delta P_{Tie}(t) \tag{7}$$

$$\Delta\dot{P}_{t2}(t) = -\frac{1}{T_{t2}}\Delta P_{t2}(t) + \frac{1}{T_{t2}}\Delta P_{g2}(t) \tag{8}$$

$$\Delta\dot{P}_{g2}(t) = -\frac{1}{R_2 T_{g2}}\Delta f_2(t) - \frac{1}{T_{g2}}\Delta P_{g2}(t) + \frac{1}{T_{g2}}\int ACE_2(t) + \frac{1}{T_{g2}}u_2(t) \tag{9}$$

$$\int \dot{ACE}_2(t) = B_2\Delta f_2(t) + \Delta P_{Tie}(t) \tag{10}$$

$$\Delta\dot{P}_{PV}(t) = -\frac{1}{T_{PV}}\Delta P_{PV}(t) + \frac{1}{T_{PV}}\Delta P_S(t) \tag{11}$$

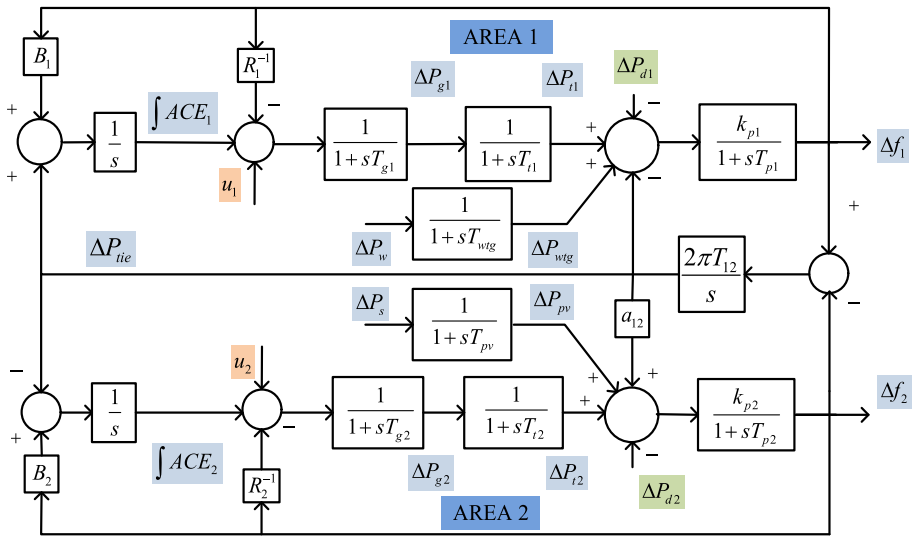

Figure 1: Structure of a 2-area LFC System

The large-scale interconnected system can be represented in state space form as follows.

$$\begin{aligned} \dot{x}(t) &= Ax(t) + Bu(t) + Dw(t) \\ y(t) &= Cx(t) + D_{yw}w(t) \\ z(t) &= C_z x(t) + D_{zu}u(t) + D_{zw}w(t) \end{aligned} \tag{12}$$

where, the state vector is denoted as $x(t) \in \Re^{11}$, the control input vector as $u(t) \in \Re^2$, the output vector as $y(t) \in \Re^2$, and the disturbance vector as $w(t) \in \Re^4$. The specific definitions for these vectors are provided in (13).

$$\begin{aligned} x(t) &= \left[\Delta f_1, \Delta P_{t1}, \Delta P_{g1}, \int ACE_1, \Delta P_{WTG}, \Delta P_{Tie}, \Delta f_2, \Delta P_{t2}, \Delta P_{g2}, \int ACE_2, \Delta P_{PV}\right], \\ y(t) &= \left[\int ACE_1, \int ACE_2\right], \\ z(t) &= \left[\Delta f_1, \int ACE_1, \Delta P_{Tie}, \Delta f_2, \int ACE_2\right] \\ w(t) &= [\Delta P_{D1} \quad \Delta P_W \quad \Delta P_{D2} \quad \Delta P_S]^T, \\ u(t) &= [u_1 \quad u_2]^T, \end{aligned} \tag{13}$$

The SOF control law for the system (12) is

$$u = Ky(t) \tag{14}$$

The closed-loop system is given by

$$\begin{bmatrix} \overline{x(t)} \\ z(t) \end{bmatrix} = \begin{bmatrix} \overline{A} & \overline{B} \\ \overline{C} & \overline{D} \end{bmatrix} \begin{bmatrix} \overline{x(t)} \\ w(t) \end{bmatrix} \tag{15}$$

where

$$\begin{aligned} \overline{A} &= A + BKC & \overline{B} &= D + BKD_{yw} \\ \overline{C} &= C_z + D_{zu}KC & \overline{D} &= D_{zw} + D_{zu}KD_{yw} \end{aligned}$$

The closed-loop transfer function matrix from $w(t)$ to $z(t)$ is

$$T_{zw}(s) = \overline{C}(sI - \overline{A})^{-1}\overline{B} + \overline{D} \tag{16}$$

3 H_∞ Controller Design

The controller design presented in this section is motivated from the design in [22]. The design considers combination of circle and strip regions LMI regions instead of conic regions in [22]. The following lemmas related to H_∞ performance (16) are taken from [22] and presented here without proof for establishing the main result.

Lemma 1 [22]. *The following statements are equivalent to $\gamma > 0$.*

1. *$\|T_{zw}(s)\| < \gamma$ and $\overline{A}$ is Hurwitz.*
2. *There exists $X = X^T > 0$ satisfying*

$$\begin{bmatrix} \mathrm{Sym}\left\{\overline{A}X\right\} & * & * \\ \overline{B}^T & -\gamma^2 I & * \\ \overline{C}X & \overline{D} & -I \end{bmatrix} < 0 \tag{17}$$

Condition (17) is BMIs due to the involvement of the term $BKCX$.

Lemma 2 [22]. *For the matrices L, M, N and O of appropriate dimensions, the condition*

$$\begin{bmatrix} L & M^T O^T \\ OM & -O - O^T + N \end{bmatrix} < 0 \tag{18}$$

implies

$$L + M^T N M < 0 \tag{19}$$

Lemma 3 [22]. *For arbitrary matrices S, T and $V = V^T > 0$, the following holds:*

$$ST + T^T S^T \leq SVS^T + T^T V^{-1} T \tag{20}$$

3.1 Decomposition of X

The following statements about matrices $Q \in \mathcal{N}(C)$ and $R \in \mathcal{R}(C)$, where $\mathcal{N}(\cdot)$ represents the null-space and $\mathcal{R}(\cdot)$ denotes the range-space, are straightforward.

1. Any matrix X can be decomposed as

$$X = \begin{bmatrix} Q^T \\ R^T \end{bmatrix}^T \begin{bmatrix} X_Q & X_S \\ X_S^T & X_R \end{bmatrix} \begin{bmatrix} Q^T \\ R^T \end{bmatrix}, \text{with} \begin{bmatrix} X_Q & X_S \\ X_S^T & X_R \end{bmatrix} > 0 \tag{21}$$

where $X_Q \in \Re^{(n-p)\times(n-p)}$, $X_S \in \Re^{(n-p)\times p}$ and $X_R \in \Re^{p\times p}$. Since $CQ = 0$, $CR = 1$, and $X = QX_QQ^T + RX_S^TQ^T + QX_SR^T + RX_RR^T$, one obtains

$$CX = X_S R^T + X_S^T Q^T \tag{22}$$

2. For all K and X, there exist an invertible matrix $X_R \in \mathbb{R}^{p\times p}$ and a matrix $Y_R \in \mathbb{R}^{m\times p}$ such that the following decomposition holds

$$KCX = Y_R R^T + Y_R X_R^{-1} X_S^T Q^T \tag{23}$$

with

$$KX_R = Y_R \tag{24}$$

Lemma 4 [22]. *The stability of system (12) with controller and the assurance of performance $||T_{zw}(s)|| < \gamma$ are guaranteed if there exist scalars ρ_1 and ρ_2. This existence is contingent upon matrices $X_Q = X_Q^T$, $X_R = X_R^T$, $Z_R = Z_R^T$, alongside X_S and Y_R satisfying the following LMI:*

$$\begin{bmatrix} \Psi_1 & * & * & * & * \\ \Psi_2 & -\gamma^2 I & * & * & * \\ \Psi_3 & D_{zw} & -I & * & * \\ \Psi_4^T & 0 & Y_R^T D_{zu}^T & -Z_R & * \\ \rho_1 X_S^T Q^T & \rho_1 D_{yw} & 0 & 0 & -\Psi_5 \end{bmatrix} < 0, \tag{25}$$

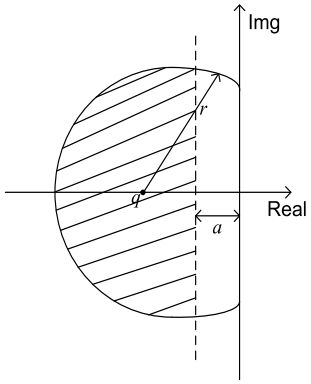

Figure 2: Regions $\mathbb{D}_{(q,r)}$ and $\mathbb{H}_a$

$$\begin{bmatrix} X_Q & X_S \\ X_S^T & X_R \end{bmatrix} > 0, Z_R > 0, \tag{26}$$

where

$$\begin{aligned}
\Psi_1 &= \mathrm{Sym}\left\{\Xi_1 + \Xi_2\right\} \\
\Xi_1 &= AQX_QQ^T + ARX_S^TQ^T + AQX_SR^T + ARX_RR^T, \\
\Xi_2 &= BY_RR^T - \rho_2 RX_S^TQ^T, \\
\Psi_2 &= D^T - \rho_2 D_{yw}^T R^T, \\
\Psi_3 &= C_zX + D_{zu}Y_RR^T, \\
\Psi_4 &= BY_R + \rho_2 RX_R \\
\Psi_5 &= \mathrm{Sym}\left\{\rho_1 X_R\right\} - Z_R
\end{aligned}$$

The proof of the Lemmas 1-5 are given in [22].

3.2 Pole Placement within Circular and Strip LMI Regions

Pole placement enhances the transient performance of the closed-loop system by strategically positioning the poles. This section expands the robust H_∞ performance to incorporate pole placement within circle and strip regions. The LMI region for pole placement with circular and strip regions is shown in Fig. 2. The characteristic equation related to circle region $\mathbb{D}_{(q,r)}$ is

$$f_{\mathbb{V}}(z) = \begin{bmatrix} -r & q+z \\ q+\bar{z} & -r \end{bmatrix} < 0, \tag{27}$$

Hence, the matrix inequality criterion corresponding to placing the closed-loop poles within $\mathbb{D}_{(q,r)}$

$$\begin{bmatrix} -rX & qX + \overline{A}X \\ qX + X\overline{A}^T & -rX \end{bmatrix} < 0. \tag{28}$$

Similarly, the characteristic equation and the matrix inequality associated with the strip region $\mathbb{H}_a$ are

$$f_{\mathbb{V}}(z) = z + \bar{z} + 2a < 0 \tag{29}$$

$$\mathrm{Sym}\left\{\overline{A}X\right\} + 2aX < 0 \tag{30}$$

Theorem 1. *The closed-loop poles of the system are positioned within the regions $\mathbb{D}_{(q,r)}$ and $\mathbb{H}_a$ if, for scalars α_1, α_2 there exist positive definite matrices $X_Q = X_Q^T$, $X_R = X_R^T$, and $Z_{R1} = Z_{R1}^T$,*

$Z_{R2} = Z_{R2}^T$, along with matrices X_S and Y_R, satisfying the following LMIs:

$$\begin{bmatrix} -rX & * & * & * \\ qX + \Xi_1^T + \Xi_2^T & -rX & * & * \\ 0 & \Psi_4^T & -Z_{R1} & * \\ \alpha_1 \Pi_1^T & 0 & 0 & -\Pi_2 \end{bmatrix} < 0, \tag{31}$$

$$\begin{bmatrix} \Psi_1 + 2aX & * & * \\ \Psi_4^T & -Z_{R2} & * \\ \alpha_2 \Pi_2^T & 0 & -\Pi_3 \end{bmatrix} < 0, \tag{32}$$

where

$$\Pi_2 = \text{Sym}\{\alpha_1 X_R\} - Z_{R1}$$
$$\Pi_3 = \text{Sym}\{\alpha_2 X_R\} - Z_{R2}$$

3.3 Parameter Tuning Using PSO

In this section, an algorithm for tuning the scalar parameters in the LMI is presented. For a large-scale system, an algorithm like `fminsearch` cannot provide a feasible solution due to the necessity of a large search space. Therefore, a metaheuristic approach, PSO, is chosen because of its advantages, such as its ability to handle high-dimensional search spaces and its robustness against local minima. The appropriate selection of the parameters ρ_1, ρ_2, α_1, and α_2 is essential for stabilizing the system and improving the transient performance through effective pole placement. The pseudo-code for optimization using the PSO algorithm is summarized in Algorithm 1.

Algorithm 1 Psuedo code for optimization using the PSO algorithm

1: Initialize the PSO algorithm by selecting the parameters ρ_1, ρ_2, α_1, and α_2.
2: Obtain state space matrices $A, B, C, D_{yw}, C_z, D_{zu}, D_{zw}$ from (12) and select suitable values of q, r and a for pole placement.
3: Set the maximum number of iterations and the minimum and maximum limits of the variables for the PSO algorithm.
4: Define the objective function to minimize the disturbance attenuation parameter $G = \sqrt{\gamma}$.
5: **for** each iteration **do**
6: Run the `mincx` algorithm to find the solution that satisfies the LMI constraints of Lemma 4 (25, 26) and Theorem 1 (31, 32) for the chosen parameters from PSO.
7: **if** the obtained γ is not the least so far **then**
8: Update the parameter values.
9: **end if**
10: **end for**
11: Obtain the optimized gains after the final iteration.

4 Simulation Results

In this section, a 2-area LFC model represented in (12) is simulated with the centralized and decentralized control schemes. The closed loop system is simulated with the following model parameters given in Table 2 for the constant matrices indicated in (12) and the parameters for circular and strip regions of pole placement are $q = -13$; $r = 12.75$; $a = -0.5$. Load disturbances of $P_{d1} = 0.01p.u$ and $P_{d2} = 0.01p.u$ are considered.

4.1 Centralized control

In this section, the controller gain of the designed centralized control is obtained by solving the LMI conditions in (25) to (26) and (31), (32) using Algorithm 1. For designing a centralized control,

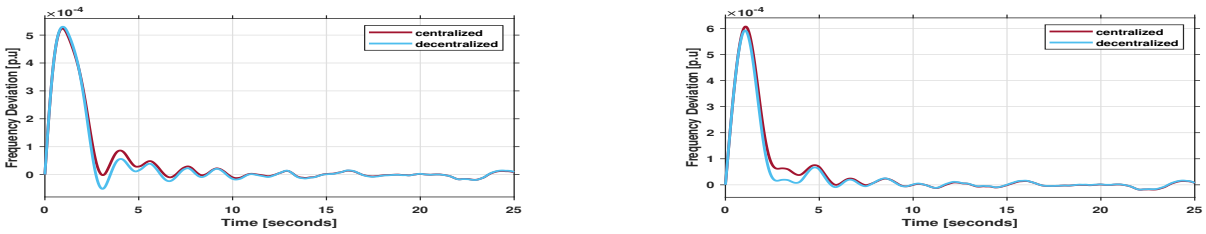

Figure 3: Comparison of Δf for centralized and decentralized controller in (a) area 1 and (b) area 2

no restrictions are needed on the matrices X_R and Y_R. The controller gain matrix K obtained for centralized control is given below.

$$K = \begin{bmatrix} -0.1626 & -0.0322 \\ 0.0823 & -0.1485 \end{bmatrix} \tag{33}$$

The pole placement parameters tuned by the PSO algorithm for centralized control are $\rho_1 = 2$, $\rho_2 = -1.2642$, $\alpha_1 = 5.2768$, and $\alpha_2 = 4.6087$.

4.2 Decentralized control

To obtain decentralized control, the same LMI conditions in (25), (26) and (31), (32) using Algorithm 1 are solved but by applying restrictions on the matrices X_R, Y_R such that the controller gain matrix K is restricted to decentralized structure. $X_R \in \mathbb{R}^{p\times p}$ is restricted to be a block diagonal matrix while $Y_R \in \mathbb{R}^{m\times p}$ is restricted to have the same structure as controller gain matrix $K \in \mathbb{R}^{m\times p}$.

The controller gain matrix K obtained for decentralized control is given below.

$$K = \begin{bmatrix} -0.1637 & 0 \\ 0 & -0.1777 \end{bmatrix} \tag{34}$$

The pole placement parameters tuned by the PSO algorithm for decentralized control are $\rho_1 = 2$, $\rho_2 = -1.0494$, $\alpha_1 = 4.2379$, and $\alpha_2 = 5.0571$.

The LFC parameters listed in Table 2 are provided in the per-unit system. Area 1 consists of two generators, each with a capacity of 500 MW, while Area 2 contains four generators, each with a capacity of 500 MW [23].

Table 2: Parameters of the LFC of a 2-area power system

Parameter	K_{pi}	T_{pi}	B_i	T_{gi}	T_{ti}	R_i	T_{WTG}	T_{PV}
Area 1	1	10	41.0	0.1	0.3	0.05	1.5	-
Area 2	0.6677	8	81.5	0.4	0.17	0.05	-	1.3

4.3 Performance of Centralized and Decentralized Controllers

In this section, the performance of centralized and decentralized controller designs are compared for stabilization and disturbance attenuation. Fig. 3 shows the frequency deviation, and Fig. 4 shows the control input of both the areas. Fig. 5 displays the disturbance attenuation γ for centralized and decentralized controllers. Here, only one output ($\int ACE(t)$) is considered per area to show that the controller can mitigate the disturbance even with fewer outputs.

4.4 Comparitive Analysis

In this section, a comparison of the designed controller with the controllers used in recent publications is presented. Table 3 shows the type of controller used and the number of outputs utilized

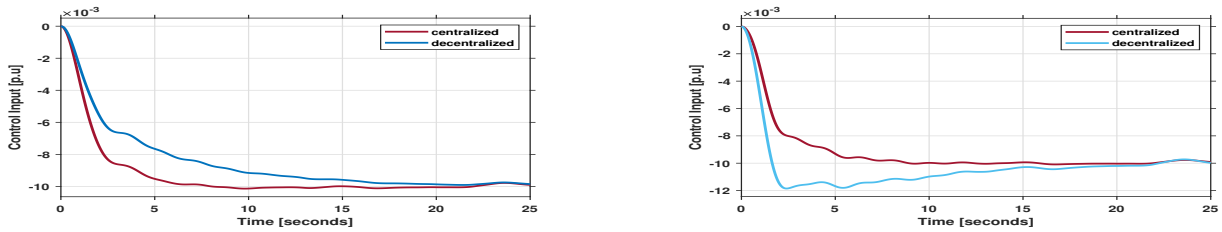

(a) (b)

Figure 4: Comparison of u_i for centralized and decentralized controller in (a) area 1 and (b) area 2

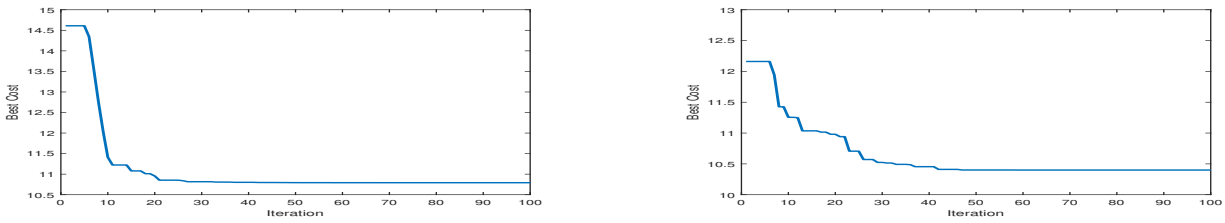

(a) (b)

Figure 5: Comparison of $\sqrt{\gamma}$ obtained from PSO for (a) centralized and (b) decentralized controllers

in the controller design. From Table 3, it can be observed that as the number of outputs increases, the controller gains also increase, which helps to improve transient performance. This is because, with more outputs, there is more flexibility in designing the controller. However, as mentioned earlier, to maintain a square matrix structure for the controller, it is only feasible to use two outputs. Consequently, in such cases, the controller gain is lower, and the disturbance attenuation is higher.

Table 3: Comparative analysis of the controllers

Controller	No. of outputs	$\|\|K\|\|$	Disturbance attenuation γ
Centralized control	2	0.1918	10.7922
Decentralized control	2	0.1777	10.4001
Overlapping [15]	5	0.59	2.56
Decentralized [14]	7	14.39	3
Centralized [9]	9	112.13	4.0124

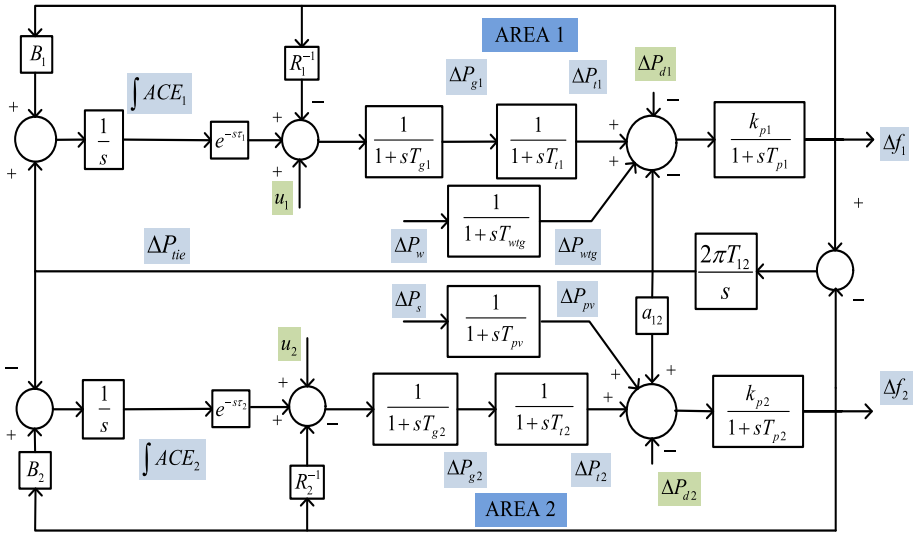

Figure 6: Structure of 2-area LFC with time delay

Table 4: Calculated maximum delay bounds for both areas

	τ_1	Maximum delay bound τ_2	Maximum delay bound τ_1	τ_2
Centralized	1	5	6	1
	2	4.75	6.05	2
	3	3.1	6.25	3
	4	2.88	2.5	4
	5	3	2.3	4.5
	6	3.42	1.5	5
Decentralized	1	3	7.9	1
	3	2.42	8.02	1.5
	5	2.77	8.2	2
	7	3.19	8.3	2.5
	8	3.31	8.4	3

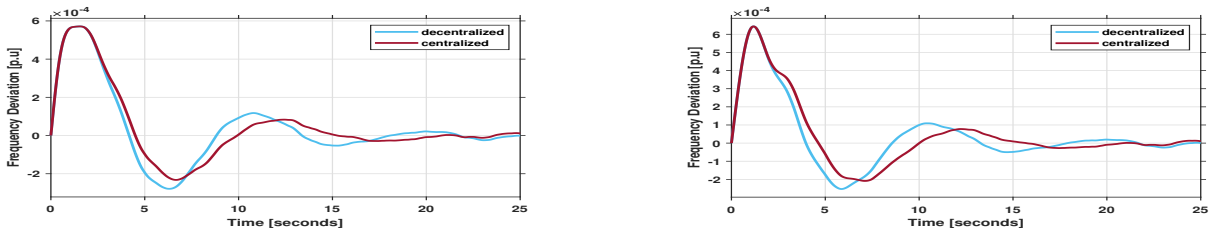

(a) (b)

Figure 7: Comparison of Δf for centralized and decentralized controller with time delays $\tau_1 = 2$ and $\tau_2 = 1.2$ seconds in (a) area 1 and (b) area 2

4.5 Robustness study with time delay

In this section, a robustness study is conducted against time delay for both centralized and decentralized control strategies. This robustness study with time delays is conducted due to the evolving nature of power systems, which are transitioning toward deregulated markets that rely on open communication networks, such as TCP/IP. In these networks, delays often arise in communication between the controller and actuator due to factors like network congestion, packet loss, and other related issues [9]. Fig. 6 shows the block diagram of the 2-area LFC scheme, incorporating time delays between the $\int ACE(t)$ signal and the actuator. Table 4, shows the delay bounds for both cases in two areas [9]. Since typical delays in LFC systems range from 2 to 4 seconds, the proposed controller demonstrates its ability to stabilize the system within these acceptable delay bounds. Fig. 7 shows the frequency deviation for both areas when time delays of $\tau_1 = 2$ seconds and $\tau_2 = 1.2$ seconds are introduced, respectively. The results indicate that the frequency deviation in the decentralized case is slightly greater than in the centralized case, although the two are relatively similar.

4.6 Robustness study with time delay and cyberattacks

In this section, the robustness of the proposed controller is analyzed in the presence of both time delays and a Man-in-the-Middle (MitM) cyberattack, specifically focusing on False Data Injection (FDI) attacks targeting the actuator.Open communication networks are vulnerable to cyberattacks, making it crucial to address these attacks and other network-related challenges. As a result, transitioning existing power systems into a Cyber-Physical Power Systems (CPPS) framework is becoming a key trend. MitM attacks are typically classified as either passive or active; passive attacks involve the attacker only monitoring data without interference, whereas active attacks involve direct manipulation of the data [25]. In this case, the study addresses an active MitM attack where the input signal, $u(t)$, is compromised by false data injection, represented as $v(t)$.

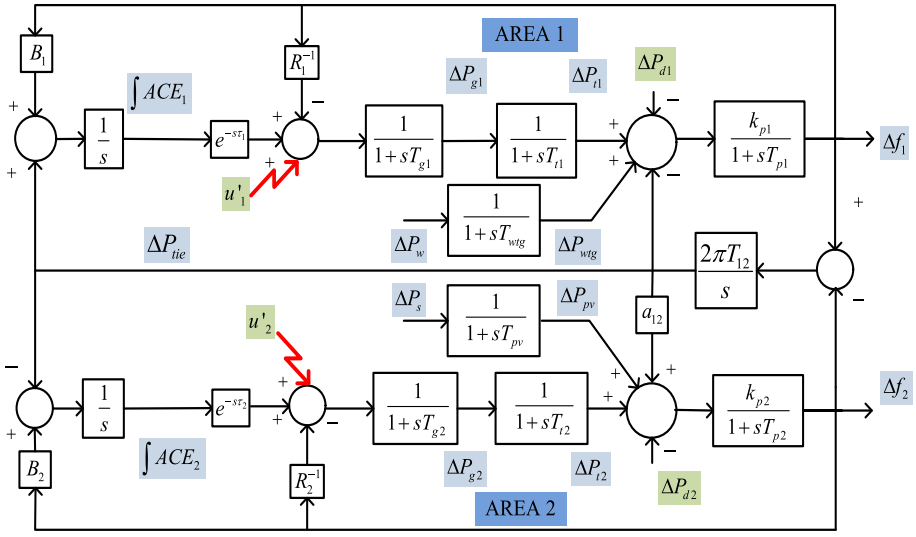

Figure 8: Structure of 2-area LFC with time delay and cyberattack

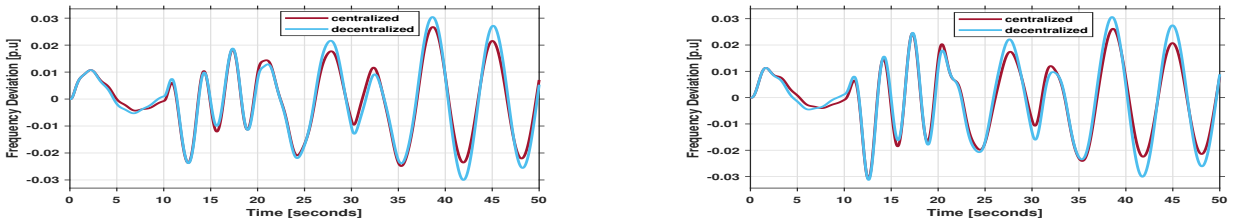

(a) (b)

Figure 9: Frequency deviation of both areas with time delays $\tau_1 = 2$ and $\tau_2 = 1.2$ seconds and deterministic cyberattack [24] for centralized and decentralized controller in (a) area 1 and (b) area 2

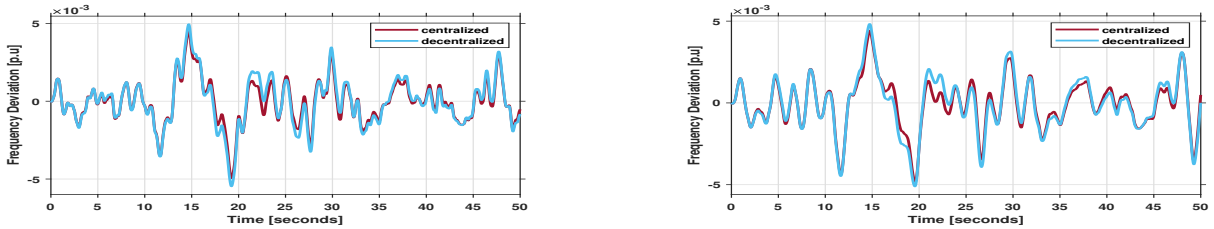

(a) (b)

Figure 10: Frequency deviation of both areas with time delays $\tau_1 = 2$ and $\tau_2 = 1.2$ seconds and stochastic cyberattack [25] for centralized and decentralized controller in (a) area 1 and (b) area 2

The manipulated control signal is expressed as:

$$u'_i(t) = u_i(t) + v_{ij}(t) \ \forall t \in [t_\ell, t_{\ell+1}) \tag{35}$$

where $v_{ij}(t)$ represents the MitM attack, treated as an input disturbance, contrasting with sensor disturbances discussed in [24]. In this analysis, both deterministic and stochastic forms of cyberattacks are considered. The case of $j = 1$ references the attack model from [24], while $j = 2$ follows the attack scenario from [25].

$$v_{i1}(t) = \begin{cases} 0.2 & 0 < t < 10 \\ 0.5sin(2t) + \frac{0.5}{t^2} & 10 < t < 20 \\ 0.2sin(t) & 20 < t < 30 \\ 0.3cos(t) & otherwise \end{cases}$$

$v_{i2}(t)$ follows the Gaussian distribution with $\mathbb{E}\{v_{i2}(t)\} = 0$ and $\mathbb{E}\{v_{i2}^2(t)\} = 1$.

Figs. 9 and 10 illustrates the frequency deviations, Δf_i $(i = 1, 2)$, in response to MitM cyberattacks. The impact of various types of cyberattacks on Δf_i is depicted in Figs. 9 and 10, demonstrating the distinct effects produced by each attack scenario.

5 Conclusion

In this work, an H_∞-based RSOF controller with regional pole placement in the LMI framework is designed for LFC of a 2-area interconnected Power System. The two key contributions of this paper are: first, a new LMI criteria employing a combination of circular and strip LMI regions for pole placement to ensure feasible controller design is proposed for large scale system and, secondly, PSO-based metaheuristic optimization algorithm is proposed with disturbance attenuation factor γ as objective function to find the feasible solution subject to various LMI constraints. Simulation results depicts that both centralized and decentralized controllers effectively stabilize the system and mitigate disturbances with only two considered outputs. The norm of the controller gain is significantly lower compared to other methods indicating that the current design uses reduced control effort. Thus, one can conclude that the modification suggested in the current design for large scale system has the potential in enhancing the performance of an interconnected power system with diverse energy sources. The designed controller when tested with with time-delay and cyberattacks, it is found that the controller is robust enough to deal with stability and disturbance rejection. In future, decentralized control design with rectangular structure of output matrices for large scale system will be attempted.

Appendix: Proof of Theorem 1

The matrix inequality given in (28) can be written as

$$\begin{bmatrix} -rX & qX + \overline{A}X \\ qX + X\overline{A}^T & -rX \end{bmatrix} = \begin{bmatrix} -rX & qX + \Xi_1 + \Xi_2 \\ qX + \Xi_1^T + \Xi_2^T & -rX \end{bmatrix} + \begin{bmatrix} 0 & \Psi_4 X_R^{-1} X_S^T Q^T \\ QX_S X_R^{-1} \Psi_4^T & 0 \end{bmatrix} \tag{36}$$

The second part of the RHS of (36) can be rewritten as follows

$$\begin{bmatrix} 0 & \Psi_4 X_R^{-1} X_S^T Q^T \\ QX_S X_R^{-1} \Psi_4^T & 0 \end{bmatrix} = \begin{bmatrix} 0 \\ \Psi_4 \end{bmatrix} X_R^{-1} \begin{bmatrix} QX_S \\ 0 \end{bmatrix}^T + \begin{bmatrix} QX_S \\ 0 \end{bmatrix} X_R^{-1} \begin{bmatrix} 0 \\ \Psi_4 \end{bmatrix}^T \tag{37}$$

Setting

$$U = \begin{bmatrix} 0 \\ \Psi_4 \end{bmatrix} X_R^{-1}, \quad V = \begin{bmatrix} X_S^T Q^T & 0 \end{bmatrix}, W = X_R Z_{R1}^{-1} X_R,$$

using Lemma 3, (37) can be rewritten as,

$$\begin{bmatrix} 0 & \Psi_4 X_R^{-1} X_S^T Q^T \\ QX_S X_R^{-1} \Psi_4^T & 0 \end{bmatrix} \leq \begin{bmatrix} 0 \\ \Psi_4 \end{bmatrix} (Z_{R1}^{-1}) \begin{bmatrix} 0 \\ \Psi_4 \end{bmatrix}^T + \begin{bmatrix} QX_S \\ 0 \end{bmatrix} \left(X_R^{-1} Z_{R1} X_R^{-1} \right) \begin{bmatrix} QX_S \\ 0 \end{bmatrix}^T \tag{38}$$

Substituting (38) in (36) and using Schur compliment

$$\begin{aligned} &\begin{bmatrix} -rX & qX + \overline{A}X \\ qX + X\overline{A}^T & -rX \end{bmatrix} \\ &= \begin{bmatrix} -rX & qX + \Xi_1 + \Xi_2 \\ qX + \Xi_1^T + \Xi_2^T & -rX \end{bmatrix} + \begin{bmatrix} 0 \\ \Psi_4 \end{bmatrix} (Z_{R1}^{-1}) \begin{bmatrix} 0 \\ \Psi_4 \end{bmatrix}^T + \begin{bmatrix} QX_S \\ 0 \end{bmatrix} \left(X_R^{-1} Z_{R1} X_R^{-1} \right) \begin{bmatrix} QX_S \\ 0 \end{bmatrix}^T \\ &= \begin{bmatrix} -rX & * & * \\ qX + \Xi_1 + \Xi_2 & -rX & * \\ 0 & \Psi_4^T & -Z_{R1} \end{bmatrix} + \begin{bmatrix} \Pi_1 \\ 0 \\ 0 \end{bmatrix} \begin{bmatrix} X_R^{-1} Z_{R1} X_R^{-1} \end{bmatrix} \begin{bmatrix} \Pi_1 \\ 0 \\ 0 \end{bmatrix}^T \end{aligned} \tag{39}$$

Using Lemma 2 and substituting the following leads to deriving the LMI associated with the circular region given in (31).

$$L = \begin{bmatrix} -rX & * & * \\ qX + \Xi_1 + \Xi_2 & -rX & * \\ 0 & \Psi_4^T & -Z_{R1} \end{bmatrix}; M^T = \begin{bmatrix} \Pi_1 \\ 0 \\ 0 \end{bmatrix} X_R^{-1}; \quad N = Z_{R1}; \quad O_1 = \alpha_1 X_R;$$

Similarly, the same procedure can obtain the LMI for the strip region as presented in (32).

References

[1] Liu, J. Z.; Qu, Q. L.; Yang, H. Y.; Zhang, J. M.; Liu, Z. D. (2024). Deep learning-based intelligent fault diagnosis for power distribution networks. *International Journal of Computers, Communications and Control*, 19(4), 5–9.

[2] Zhao, X.; Ma, Z.; Li, S.; Zou, S. (2022). Robust LFC of power systems with wind power under packet losses and communication delays. *IEEE Journal on Emerging and Selected Topics in Circuits and Systems*, 12(1), 135–148.

[3] Jagatheesan, K.; Anand, B.; Dey, N.; Ashour, A. S.; Barna, C.; Balas, V. E. (2016). Automatic generation control of an interconnected multi-area reheat thermal power systems with conventional proportional-integral controller considering various performance indices. In *2016 IEEE 11th International Symposium on Applied Computational Intelligence and Informatics (SACI)*, pages 289–294.

[4] Van, H. V.; Minh, B. L. N.; Amaefule, E. N.; Tran, A. T.; Tran, P. T.; Van-Duc, P.; Pham, V. T.; Nguyen, T. M. (2021). Load frequency control for multi-area power plants with integrated wind resources. *Applied Sciences (Switzerland)*, 11(7), 1–9.

[5] Lv, X.; Sun, Y.; Hu, W.; Dinavahi, V. (2021). Robust load frequency control for networked power system with renewable energy via fractional-order global sliding mode control. *IET Renewable Power Generation*, 15(5), 1046–1057.

[6] Ansari, J.; Abbasi, A. R.; Firouzi, B. B. (2022). Decentralized LMI-based event-triggered integral sliding mode LFC of power systems with disturbance observer. *International Journal of Electrical Power and Energy Systems*, 138, 1–10.

[7] Khamies, M.; Magdy, G.; Kamel, S.; Khan, B. (2021). Optimal model predictive and linear quadratic gaussian control for frequency stability of power systems considering wind energy. *IEEE Access*, 9, 1–12.

[8] Bondalapati, S.; Dey, R.; Mekhilef, S.; Guelton, K. (2023). Linear quadratic differential games based MIMO-PID design for load frequency control of a 2-area interconnected power system: An iterative LMI approach. *IFAC-PapersOnLine*, 56(2), 348–353. 22nd IFAC World Congress.

[9] Dey, R.; Ghosh, S.; Ray, G.; Rakshit, A. (2012). H-infinity load frequency control of interconnected power systems with communication delays. *International Journal of Electrical Power and Energy Systems*, 42, 672–684.

[10] Dhillon, S. S.; Lather, J. S.; Marwaha, S. (2016). Multi objective load frequency control using hybrid bacterial foraging and particle swarm optimized PI controller. *International Journal of Electrical Power & Energy Systems*, 79, 196–209.

[11] Barakat, M.; Donkol, A.; Hamed, H. F. A. (2021). Harris hawks-based optimization algorithm for automatic LFC of the interconnected power system using PD-PI cascade control. *J. Electr. Eng. Technol.*, 16, 1845–1865.

[12] Saka, M.; Gozde, H.; Eke, I.; Taplamacioglu, M. C. (2022). Neural network based heuristic fractional order adaptive PID-controller for eliminating communication time delay in multi-area LFC. *International Journal of Numerical Modelling: Electronic Networks, Devices and Fields*, 35(6), e3021.

[13] Simhadri, K. S.; Mohanty, B. (2019). Performance analysis of dual-mode PI controller using quasi-oppositional whale optimization algorithm for load frequency control. *International Transactions on Electrical Energy Systems*, 30(1), e12159.

[14] Ahmadi, A.; Aldeen, M. (2016). An LMI approach to the design of robust delay-dependent overlapping load frequency control of uncertain power systems. *International Journal of Electrical Power and Energy Systems*, 81, 48–63.

[15] Ahmadi, A.; Aldeen, M. (2017). Robust overlapping load frequency output feedback control of multi-area interconnected power systems. *International Journal of Electrical Power and Energy Systems*, 89, 156–172.

[16] Jerbi, H.; Kchaou, M.; Alshammari, O.; Abassi, R.; Popescu, D. (2022). Observer-based feedback control of interval-valued fuzzy singular system with time-varying delay and stochastic faults. *International Journal of Computers, Communications and Control*, 17(6), 1–9.

[17] Pradhan, S. K.; Das, D. K. (2022). H-infinity controller design for frequency control of delayed power system with actuator saturation and wind source integration. *Arabian Journal for Science and Engineering*, 47(11), 13873–13891.

[18] Oshnoei, A.; Kheradmandi, M.; Muyeen, S. M. (2020). Robust control scheme for distributed battery energy storage systems in load frequency control. *IEEE Transactions on Power Systems*, 35(6), 4781–4791.

[19] Singh, V. P.; Kishor, N.; Samuel, P. (2017). Improved load frequency control of power system using LMI based PID approach. *Journal of the Franklin Institute*, 354(15), 6805–6830.

[20] Arunagirinathan, S.; Muthukumar, P.; Yu, S. S.; Trinh, H. (2021). A novel observer-based approach to delay-dependent LFC of power systems with actuator faults and uncertain communications conditions. *International Journal of Electrical Power and Energy Systems*, 131, 1–9.

[21] Sadabadi, M. S.; Peaucelle, D. (2016). From static output feedback to structured robust static output feedback: A survey. *Annual Reviews in Control*, 42, 11–26.

[22] Sahoo, P. R.; Goyal, J. K.; Ghosh, S.; Naskar, A. K. (2019). New results on restricted static output feedback H-infinity controller design with regional pole placement. *IET Control Theory and Applications*, 13(8), 1095–1104.

[23] Kundur, P. (1994). *Power System Stability and Control*. New York: McGraw-Hill, 581–623.

[24] Saxena, S.; Fridman, E. (2020). Event-triggered load frequency control via switching approach. *IEEE Transactions on Power Systems*, 35, 4484–4494.

[25] Kumar, R.; Dey, R.; Guelton, K.; Bali, A.; Singh, U. P. (2024). Adaptive control for cyber-physical systems under man-in-the-middle attacks with false data injections. *Journal of the Franklin Institute*, 361(4), 1–10.

Journal's webpage: http://univagora.ro/jour/index.php/ijccc/

This journal is a member of, and subscribes to the principles of,
the Committee on Publication Ethics (COPE).
https://publicationethics.org/members/international-journal-computers-communications-and-control

Cite this paper as:

Bondalapati, S.; Dey, R.; Barna, C.; Balas V.E (2024). H_∞- Static Output Feedback based Load Frequency Control of an Interconnected Power System with Regional Pole Placement, *International Journal of Computers Communications & Control*, 19(6), 6857, 2024.
https://doi.org/10.15837/ijccc.2024.6.6857